ATLAS NOTE

ATLAS-CONF-2015-029

23rd July 2015

Selection of jets produced in 13 TeV proton-proton collisions with the ATLAS detector

The ATLAS Collaboration

Abstract

Quality criteria for the selection of reconstructed $R = 0.4$ anti-kt jets with ATLAS are described. The study is based on $\sqrt{s} = 13$ TeV proton–proton collision data recorded in June 2015 by the ATLAS detector at the Large Hadron Collider. Two selection criteria are introduced. The Loose selection is designed to provide an efficiency of selecting jets from proton-proton collisions above 99.5% (99.9%) for $p_{\mathrm{T}} > 20$ (100) GeV to be used in most ATLAS physics analyses. A tighter set of selection cuts, called Tight, is designed to further reject background jets for analyses sensitive to non-collision backgrounds with an efficiency of selecting jets from proton-proton collisions above 95% (99.5%) for $p_{\mathrm{T}} > 20$ (100) GeV.

ATLAS-CONF-2015-029
25 July 2015

1 Introduction

Jets at high transverse momenta produced in proton-proton collisions must be distinguished from misidentified jets of non-collision origin. This note summarizes the selection criteria recommended to identify jets originating from proton-proton collisions produced by the Large Hadron Collider (LHC), with a centre-of-mass energy of $\sqrt{s}$ = 13 TeV, recorded in 2015 with the ATLAS detector. It updates the earlier studies described in References [1, 2].

The main backgrounds for jets coming from collision events are the following:

1. Beam induced background (BIB) due to proton losses upstream of the interaction point. These proton losses induce secondary cascades leading to muons that can reach the ATLAS detector and become a source of background for physics analyses [1]. The energy depositions created by these muons can be reconstructed as fake jets with energy as high as the beam energy. The rate of BIB is proportional to the beam current and depends on the operational conditions of the LHC, such as machine optics, collimator settings, residual gas densities, and filling scheme.

2. Cosmic-ray showers produced in the atmosphere overlapping with collision events. Since ATLAS is deep underground, the particles reaching the ATLAS detector are predominantly muons.

3. Calorimeter noise from large scale coherent noise or isolated pathological cells. Calorimeter cells which are permanently or sporadically very noisy are masked[1] prior to the jet and missing transverse momentum reconstruction. The former is always masked in the event reconstruction, while the sporadically very noisy cells are masked on an event-by-event basis. Events are discarded if they are identified as having a large amount of coherent noise. Most of the noise is already identified and rejected by the data quality inspection [3] performed shortly after the data taking based on standardised quality criteria. A small fraction of calorimeter noise remains undetected and needs to be rejected by additional criteria.

The two first sources of background are referred to as non-collision backgrounds.

The jet selection criteria should efficiently reject jets from background processes while keeping the highest efficiency selection for jets produced in proton-proton collisions. Since the level and composition of background depend on the jet multiplicity and the jet kinematics, two sets of criteria are proposed that each correspond to different levels of fake jet rejection and jet selection efficiency. Jet candidates arising as high energy objects produced in a collision event are called “good jets”, while jet candidates coming from background processes are called “fake jets”. The study presented in this document limits its scope to anti-k_t $R = 0.4$ jets.

An overview of the ATLAS detector and its calorimeter system is provided in Section 2. Data samples used in this note are presented in Section 3 and jet reconstruction is specified in Section 4. Details of the jet selection are provided in Section 5 and the jet quality criteria are presented in Section 6. Section 7 presents in-situ measurements of the jet selection efficiency.

[1] The fraction of cells permanently masked is smaller than one per mil and the fraction of cells that are conditionally masked is smaller than one per mil.

2 The ATLAS detector

The ATLAS experiment [4] is a multipurpose particle physics detector with a forward-backward symmetric cylindrical geometry.[2]. It covers almost the whole solid angle around the collision point with layers of tracking detectors (up to $|\eta| = 2.5$), calorimeters (up to $|\eta| = 4.9$), and muon chambers (up to $|\eta| = 2.7$)

The inner detector (ID) is used to reconstruct tracks from the passage of charged particles. The ID has complete azimuthal coverage and spans the region $|\eta| < 2.5$. It consists of layers of high-granularity silicon pixel detectors, silicon microstrip detectors and transition radiation tracking detectors. A solenoid magnet provides a uniform magnetic field of 2 T inside the tracking detectors, generating track curvature which can be used to determine charged particle momenta.

For the measurements presented in this paper, the calorimeter system is of particular importance. High granularity liquid-argon electromagnetic sampling calorimeters (LAr) cover the pseudorapidity range $|\eta| < 3.2$. The hadronic calorimetry in the range $|\eta| < 1.7$ is provided by a scintillator-tile calorimeter (Tile), which is separated into a central barrel and two smaller extended barrel cylinders, one on either side of the central barrel. In the end-caps ($|\eta| > 1.5$), the LAr technology is also used for the hadronic calorimeters (HEC), matching the outer $|\eta|$ limits of the electromagnetic end-cap calorimeters. The LAr forward calorimeters (FCal) extend the coverage to $|\eta| = 4.9$ with electromagnetic and hadronic energy measurements.

3 Data and Monte Carlo samples

3.1 Data

The dataset consists of proton-proton collisions at a centre-of-mass energy of $\sqrt{s} = 13$ TeV, recorded in June 2015. Requirements to ensure the quality of beam conditions, detector performance and data are imposed [3, 5]. After application of these criteria, the total integrated luminosity is 6.4 ± 0.6 pb^{-1}.

3.2 Simulation of dijet events

The jet selection efficiency measurement is compared to Monte Carlo simulation. Samples of inclusive dijet events from strong interaction processes are generated with Pythia8 [6] using the NNPDF23LO parton distribution functions (PDFs). Additional radiation is modeled using p_T-ordered parton showers [7]. Parton fragmentation and hadronization is modelled using the Lund string model [8]. These predictions are produced using the A14 [9] tune for underlying event activity.

Generated events are propagated through a full simulation of the ATLAS detector [10] based on Geant4 [11] that simulates the particle interactions with the detector material. Hadronic showers are simulated with the FTFP BERT model [12]. Different pile-up (multiple proton–proton interactions in the same or neighbouring bunch-crossings) conditions as a function of the instantaneous luminosity are taken into account by overlaying simulated minimum bias events generated with Pythia8 onto the hard-scattering

[2] ATLAS uses a right-handed coordinate system with its origin at the nominal interaction point in the centre of the detector and the z-axis along the beam pipe. Cylindrical coordinates (r, ϕ) are used in the transverse plane, ϕ being the azimuthal angle around the beam pipe. The pseudorapidity η is defined in terms of the polar angle θ as $\eta = -\ln\tan(\theta/2)$.

process and reweighting them according to the distribution of the mean number of interactions observed in data.

4 Event reconstruction

Jet candidates are reconstructed using the anti-k_t jet clustering algorithm [13] with a distance parameter of $R = 0.4$. The inputs to this algorithm are topologically connected clusters of calorimeter cells (topo-clusters) [2], seeded by cells with energy significantly above the measured noise. These topoclusters are at the electromagnetic (EM) energy scale, which correctly measures the energy deposited by electromagnetic showers in the calorimeter. Jets are corrected for the effects of calorimeter non-compensation and inactive material by using energy and η-dependent calibration factors, based on Monte Carlo simulation and collision-data [2, 14]. Additional corrections are applied to the jets to reduce the dependence of the jet energy measurement on the longitudinal and transverse structure of the jets and also to correct for jets that are not fully contained in the calorimeter.

Tracks used in this study are reconstructed within the full acceptance of the ID ($|\eta| < 2.5$) from individual hits of charged particles in the ID sub-detectors [15]. Tracks are required to have transverse momentum of at least 500 MeV, in addition to quality criteria relating to impact parameters and numbers of hits in the different ID sub-detectors [14]. Tracks should either be used in the fit to the selected primary vertex or have the longitudinal impact parameter with respect to the primary vertex satisfying $|z_0 \sin\theta| < 3.0\,\text{mm}$. Tracks are associated to jets using ghost association [16] that treats them as 4-vectors of infinitesimal magnitude during jet reconstruction.

5 Event selection

The criteria for the jet quality selection are optimized by studying two different event samples, one enriched with good and the other with fake jets:

- Good jets are selected by requiring that the two leading jets have $p_{\text{T}} > 70$ GeV and are back-to-back ($\Delta\phi_{j-j} > 3.0$ radians) in the plane transverse to the beam. The two jets are required to be balanced in transverse momentum ($|{p_{\text{T}}}^1 - {p_{\text{T}}}^2|/({p_{\text{T}}}^1 + {p_{\text{T}}}^2) < 0.3$). Events are selected with single jet triggers.[3] For each p_{T}-bin considered in this analysis, a dedicated trigger chain is chosen that is fully efficient (> 99%) while having a prescale factor as small as possible. This sample is dominated by dijet events produced by strong interactions and will henceforth be referred to as the "good jets enriched sample".
- Fake jets are selected from events with at least one jet with $p_{\text{T}} > 70$ GeV. Since events with fake jets are characterized by jets with unbalanced transverse momentum, only events satisfying $H_{\text{T}}^{\text{miss}} = |\overrightarrow{H}_{\text{T}}^{\text{miss}}| > 70$ GeV are retained. The variable $\overrightarrow{H}_{\text{T}}^{\text{miss}}$ is defined as $\overrightarrow{H}_{\text{T}}^{\text{miss}} = -\sum_{\text{jets}} \overrightarrow{p_{\text{T}}}$ where all jets with p_{T} greater than 20 GeV are considered. In addition, the direction of $\overrightarrow{H}_{\text{T}}^{\text{miss}}$ should be

[3] In order to select jets with $p_{\text{T}} > 70$ GeV, two single jet triggers are considered with different online jet p_{T} thresholds. The one with the high threshold is fully efficient to select offline jets with $p_{\text{T}} > 270$ GeV while the one with the low threshold is fully efficient to select offline jets with $p_{\text{T}} > 70$ GeV. Due to its high rate, the lowest threshold trigger is prescaled by a factor of about 10. In all distributions presented in this document, the data recorded by this trigger are normalised taking into account the prescale correction.

opposite to the transverse component of the jet momentum ($\Delta\phi_{H_{\mathrm{T}}^{\mathrm{miss}}-j} > 3.0$ radians). In order to reduce the contribution from physics processes like $Z(\rightarrow \nu\nu)$+jets, the leading jet is required to be out-of-time ($|t_{\mathrm{jet}}| > 6$ ns), where the jet time (t_{jet}) is defined by the energy–squared weighted average of the time of the energy deposits in the jet: $t_{\mathrm{jet}} = \sum E_{\mathrm{cell}}^2 t_{\mathrm{cell}} / \sum E_{\mathrm{cell}}^2$ where the sum runs over the cells belonging to the jet. Jets produced in proton-proton collisions are expected to be reconstructed at $t_{\mathrm{jet}} = 0$. This jet sample is dominated by non-collision backgrounds described in Section 1, and will henceforth be referred to as the "fake jets enriched sample". The jet triggers used for the good jets samples are also used to select these jets.

6 Description of the quality criteria

6.1 Jet quality variables

Several variables were introduced to discriminate fake and good jets in References [1, 2] and they can be divided into three categories: variables based on signal pulse shape in the LAr calorimeters[4], energy ratio variables, and track-based variables. Pulse shape variables provide good discrimination against noise in the LAr calorimeters. The energy ratio variable and track-based variables are effective at rejecting calorimeter noise in the LAr and Tile calorimeters, in addition to rejecting beam-induced background and cosmic muon showers.

6.1.1 Discriminating variables for calorimeter noise

In order to reject fake jets due to significant coherent or sporadic noise in the LAr calorimeters, the characteristic ionisation signal shape can be used to discriminate between real and fake energy deposits. The measured pulse in a given LAr calorimeter cell is compared to the expected pulse shape from simulation of the electronics response, and the quadratic difference $Q_{\mathrm{cell}}^{\mathrm{LAr}}$ between the actual and expected pulse shapes is used to discriminate noise from real energy deposits. $Q_{\mathrm{cell}}^{\mathrm{LAr}}$ is computed online using the four measured samples of the pulse shape:

$$Q_{\mathrm{cell}}^{\mathrm{LAr}} = \sum_{j=1}^{4} (s_j - A \cdot (g_j - \tau g'_j))^2, \tag{1}$$

where A is the measured amplitude of the signal [17], τ the measured time of the signal, s_j the amplitude of each sample, j, in ADC counts, g_j the normalized predicted ionization shape and g'_j its derivative. $Q_{\mathrm{cell}}^{\mathrm{LAr}}$ is stored as a 16-bit unsigned integer and any values above 2^{16}-1 are set to the maximum value.

From this cell-level quantity ($Q_{\mathrm{cell}}^{\mathrm{LAr}}$), several jet-level quantities are derived:

- $\langle Q \rangle$: The average jet quality is defined as the energy–squared weighted average of the pulse quality of the calorimeter cells ($Q_{\mathrm{cell}}^{\mathrm{LAr}}$) in the jet. This quantity is normalized such that $0 < \langle Q \rangle < 1$.
- $f_{\mathrm{Q}}^{\mathrm{LAr}}$: Fraction of the energy in the LAr calorimeter cells of a jet with poor signal shape quality defined as $Q_{\mathrm{cell}}^{\mathrm{LAr}} > 4000$.

[4] The LAr Calorimeters in ATLAS are calorimeters based on liquid-argon as active material and are composed of the electromagnetic calorimeter, the hadronic end-cap calorimeter and the forward calorimeter.

- $f_{\mathrm{Q}}^{\mathrm{HEC}}$: Fraction of the energy in the HEC calorimeter cells of a jet with poor signal shape quality defined as $Q_{\mathrm{cell}}^{\mathrm{LAr}} > 4000$.

Finally, since sporadically noisy cells in the calorimeter can generate large fake energy deposits as well as large fake negative energy deposits, a variable, E_{neg}, summing the energy of all cells with negative energy is introduced. The presence of negative energy in a good jet is due to the electronic and pile-up noise.

The distributions of these four variables can be found in Figure 1 in the good and fake jets enriched samples.

In the good jet enriched sample, the variables $\langle Q \rangle$, $f_{\mathrm{Q}}^{\mathrm{LAr}}$ and $f_{\mathrm{Q}}^{\mathrm{HEC}}$ have a high population of jets at zero. Values different from zero are due to electronic and pile-up noise which can distort the measured pulse shape. Non-zero values are also caused by differences in the pulse shape between data and the expectation used in Equation 1. Since the simulation uses a consistent pulse shape, it predicts values closer to zero generated only by the electronic and pile-up noise. Simulated distributions are therefore not shown for these three variables. In the fake jets enriched sample, the variables $\langle Q \rangle$, $f_{\mathrm{Q}}^{\mathrm{LAr}}$ and $f_{\mathrm{Q}}^{\mathrm{HEC}}$ contain a higher proportion of jets with larger values. Values close to one are mainly due to large coherent noise or sporadically very noisy cells in the calorimeters and intermediate values are mainly due to beam-induced background.

Most of the jets have a low value of $|E_{\mathrm{neg}}| < 50$ GeV, except a population of fake jets with $|E_{\mathrm{neg}}| > 60$ GeV which also has large values of $f_{\mathrm{Q}}^{\mathrm{HEC}}$. Those jets are mainly due to sporadic noise bursts in the HEC [2]. Good agreement is observed between data and the simulation in the good jets enriched sample at low values but discrepancies in the tails are observed where the simulation overpredicts the data.

6.1.2 Energy ratio variables

Jets originating from beam-induced background or calorimeter noise tend to be more localised longitudinally in the calorimeters than jets from proton-proton collisions. Therefore, the jet energy deposits along the expected direction of the shower development can be employed to discriminate between good jets and jets arising from non-collision backgrounds. The electromagnetic fraction (f_{EM}) is defined as the ratio of the energy deposited in the electromagnetic calorimeter to the total energy of the jet. Similarly, the HEC energy fraction (f_{HEC}) is defined as the ratio of the energy deposited in the HEC calorimeter to the total energy. The ATLAS calorimeters are segmented in depth and the maximum energy fraction in any single calorimeter layer (f_{max}) can be used as a discriminating variable between fake and good jets. All of these ratio variables are computed at the electromagnetic energy scale.

The distributions of three variables can be found in Figure 2. Figure 3 shows $f_{\mathrm{Q}}^{\mathrm{LAr}}$ as a function of the electromagnetic fraction for the fake and good jets enriched samples.

Good jets have a smooth distribution for these three variables. Jets that fall outside of the HEC acceptance exhibit a peak at $f_{\mathrm{HEC}} = 0$. The fake jets distribution has very high or very low values for both f_{EM} and f_{HEC}, and high values for f_{max}. Good agreement is observed between data and the simulation for good jets.

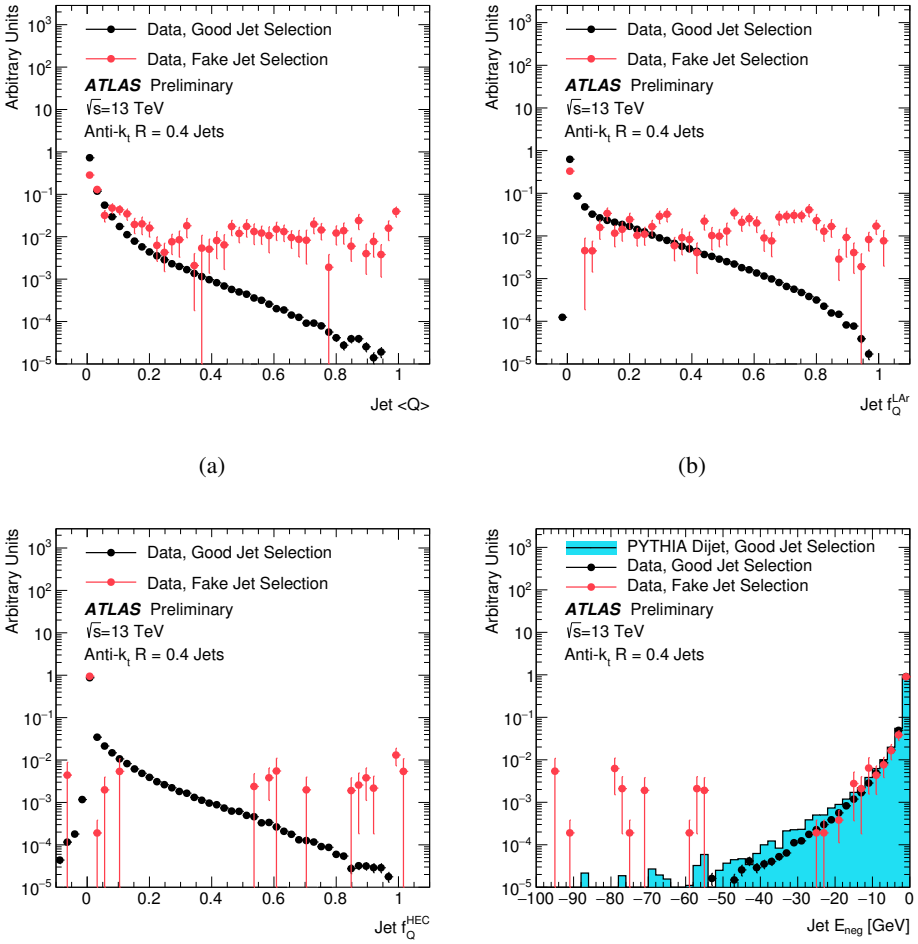

Figure 1: *Distributions of* $f_{\mathrm{Q}}^{\mathrm{LAr}}$ *(a),* $f_{\mathrm{Q}}^{\mathrm{HEC}}$ *(b),* $\langle Q \rangle$ *(c) and* E_{neg} *(d) in the good jets enriched sample for data (black points) and for the simulation (blue histogram) only shown for (d). Distributions from the fake jet enriched samples are superimposed (red points).*

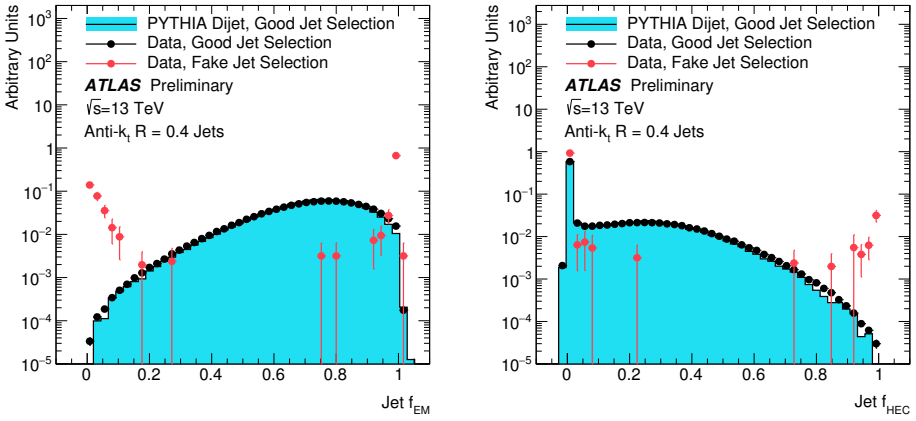

(a) (b)

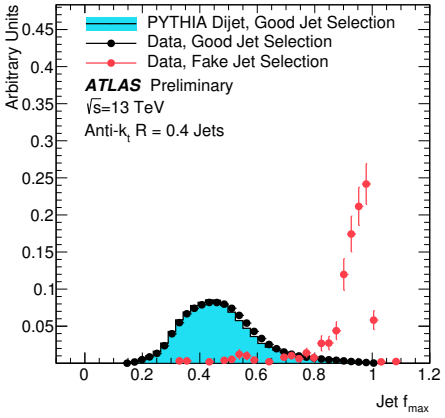

(c)

Figure 2: *Distributions of f_{EM} (a), f_{HEC} (b) and f_{max} (c) in the good jets enriched sample for both data (black points) and the simulation (blue histograms). Distributions from the fake jet enriched samples are also superimposed (red points).*

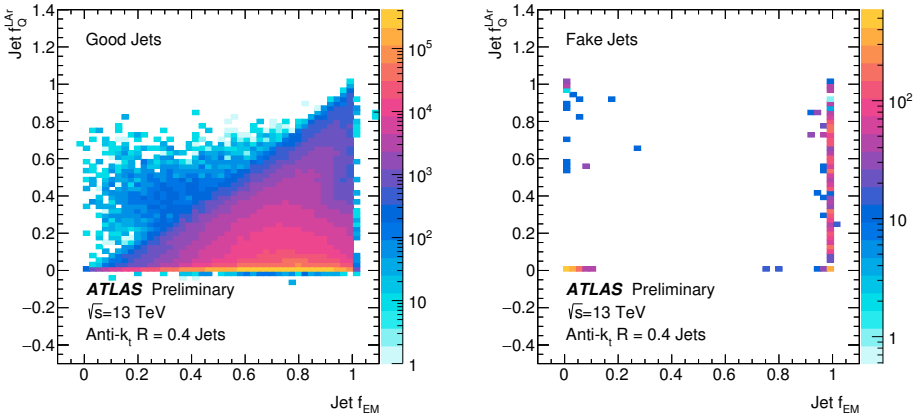

(a) (b)

Figure 3: *Distribution of $f_{\mathrm{Q}}^{\mathrm{LAr}}$ as a function of the electromagnetic fraction for the good (a) and fake (b) jets enriched samples in data.*

6.1.3 Track based variables

Most real jets contain charged hadrons which can be reconstructed by the ID tracking system for jets in the tracker acceptance. The jet charged fraction (f_{ch}) is defined as the ratio of the scalar sum of the p_{T} of the tracks coming from the primary vertex (see Section 4) associated to the jet divided by the jet p_{T}.

The ratio between the jet charged particle fraction and the jet energy fraction in the layer with maximum energy deposit ($f_{\mathrm{ch}}/f_{\mathrm{max}}$) was also found to discriminate between good and fake jets.

The distributions of these variables are given in Figure 4 for jets with $|\eta| < 2.4$ and Figure 5 shows the jet charged fraction as a function of the electromagnetic fraction for the fake and good jets enriched samples. The fake jets have low values for f_{ch} and $f_{\mathrm{ch}}/f_{\mathrm{max}}$ while only a small fraction of good jets have low values. Good agreement is observed between data and the simulation for good jets.

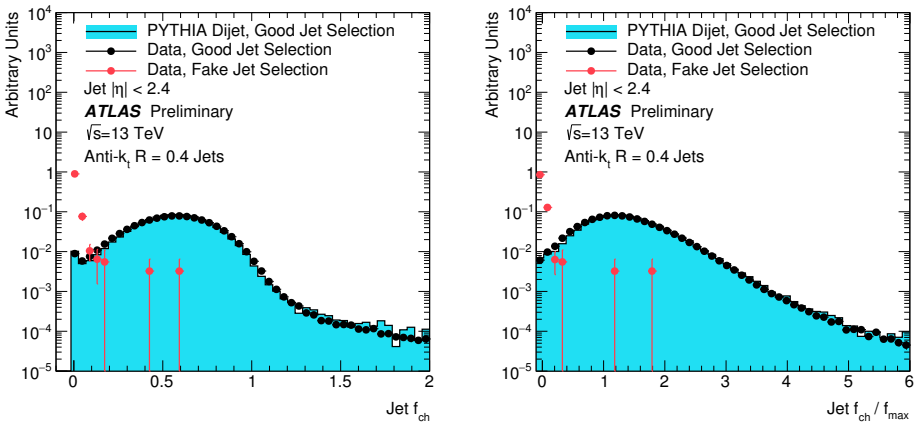

(a) (b)

Figure 4: *Distributions of f_{ch} (a) and $f_{\mathrm{ch}}/f_{\mathrm{max}}$ (b) for $|\eta|$ <2.4 in the good jets enriched sample for both data (black points) and the simulation (blue histograms). Distributions from the fake jet enriched samples are also superimposed (red points).*

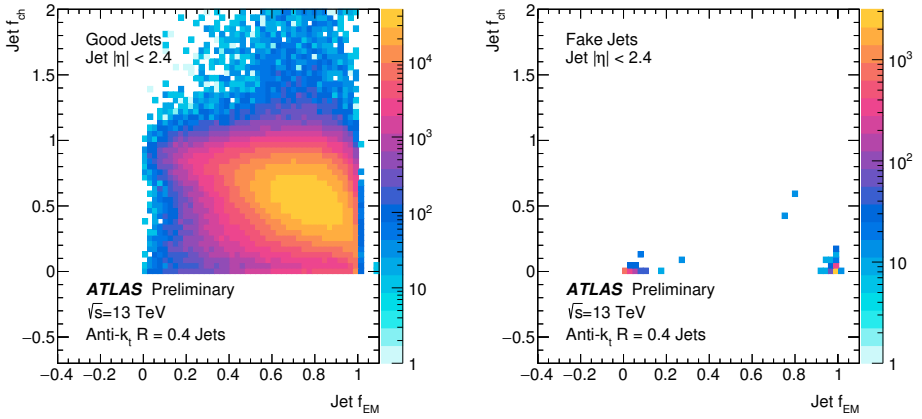

(a) Good jets (b) Fake jets

Figure 5: *Distribution of f_{ch} as a function of the electromagnetic fraction for the good (a) and fake (b) jets enriched samples in data.*

6.2 Jet quality selection

Two selections to identify fake jets are proposed, called the BadLoose and BadTight jet selections. The BadLoose selection, initially introduced in References [1, 2][5], is designed for high good jet efficiency, while maintining as high fake jet rejection as possible. A jet is identified as a BadLoose jet if it satisfies at least one of following criteria:

1. $f_{\mathrm{HEC}} > 0.5$ and $| f_{\mathrm{Q}}^{\mathrm{HEC}} | > 0.5$ and $\langle Q \rangle > 0.8$
2. $| E_{\mathrm{neg}} | > 60$ GeV
3. $f_{\mathrm{EM}} > 0.95$ and $f_{\mathrm{Q}}^{\mathrm{LAr}} > 0.8$ and $\langle Q \rangle > 0.8$ and $| \eta | < 2.8$
4. $f_{\mathrm{max}} > 0.99$ and $| \eta | < 2$
5. $f_{\mathrm{EM}} < 0.05$ and $f_{\mathrm{ch}} < 0.05$ and $| \eta | < 2$
6. $f_{\mathrm{EM}} < 0.05$ and $| \eta | \geq 2$

The first two criteria are introduced to identify jets mainly due to sporadic noise bursts in the HEC. The third selection has the purpose to identify jets due to large coherent noise or isolated pathological cells in the electromagnetic calorimeter. The last three requirements are more general and are used to identify hardware issues, beam-induced background and cosmic muon showers.

The BadTight selection is designed to provide a much higher fake jet rejection with an inefficiency for good jets of up to a few percent. It adds a single criterion which is based on the ratio between the f_{ch} and f_{max}. This ratio is very efficient at discriminating fake jets (which have preferentially f_{ch} close to 0 and f_{max} close to 1) and jets from proton-proton collisions which have preferencially $f_{\mathrm{ch}} > 0$ and $f_{\mathrm{max}} < 1$ as shown in Figure 4. A jet is identified as a BadTight jet if it is a BadLoose jet or if it satisfies: $f_{\mathrm{ch}}/f_{\mathrm{max}} < 0.1$ for $|\eta| < 2.4$.

These criteria were initially introduced in the ATLAS search for new phenomena in final states with an energetic jet and large missing transverse momentum [18]. This analysis is one of the those which needs the most restrictive jet selection due to the similar event topology of non-collision backgrounds and the final states analysed. Usage of BadTight criteria in this search reduced the non-collision backgrounds to a negligible level compared to the Standard Model backgrounds from proton-proton collisions for this analysis that is highly sensitive to calorimeter noise, beam-induced background, and cosmic muon showers.

A jet is identified as a Loose jet if it is not identified as a BadLoose jet, and a jet is identified as a Tight jet if it is not identified as a BadTight jet. Figures 6 and 7 show kinematic distributions for the fake jets enriched sample before the jet quality selection and after applying the Loose and Tight jet selections. The Tight selection provides very good rejection of the fake jet enriched sample, in particular at high jet transverse momentum. The peaks at $\phi = 0$ and $\pm\pi$, which are characteristic of beam background [1], are eliminated by the Tight selection. It should also be noted that the beam-induced background peaks at low $|\eta|$ values due to the requirements on the jet transverse momentum and the jet timing [1].

[5] This working point was called Looser in these references.

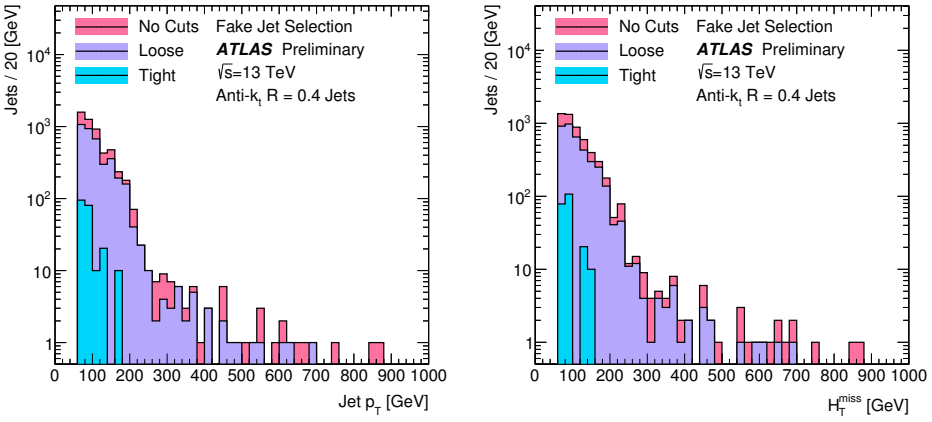

(a) (b)

Figure 6: *Jet transverse momentum (a) and $H_{\mathrm{T}}^{\mathrm{miss}}$ (b) distributions for the fake jets enriched sample before and after the jet quality selection.*

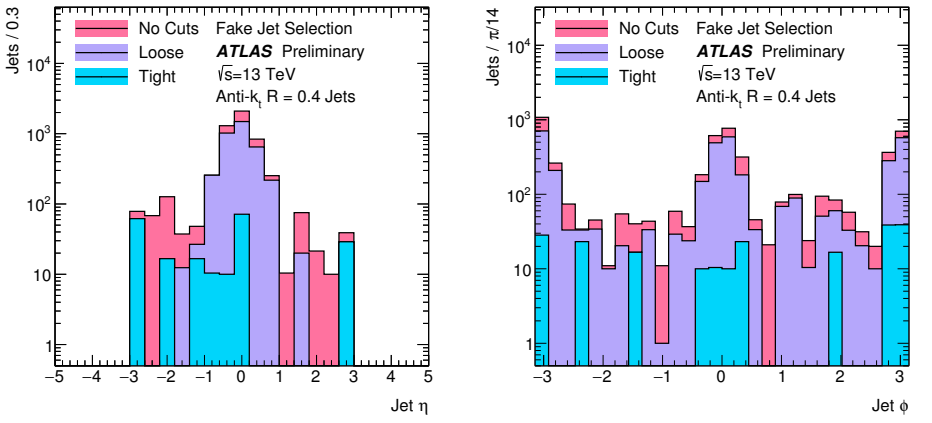

(a) (b)

Figure 7: *η (a) and ϕ (b) distributions for the fake jets enriched sample before and after the jet quality selection.*

7 Jet selection efficiency measurement

The efficiencies of the jet quality selections are measured using a "tag-and-probe" method. Good dijet events, as described in Section 5, are selected by modifying the jet transverse momentum criterion to be greater than 20 GeV instead of 70 GeV.

The tag jet is required to pass the Tight version of the jet quality selections, and to be back-to-back in the transverse plane with the probe jet. Among the two leading jets, each jet can play the role of the probe jet as long as the other jet satisfies the tag criteria. The sample of probe jets is used to measure the jet quality selection efficiency defined as the fraction of probe jets that are not rejected by the jet quality selection criteria as a function of η and p_{T} of the probe jets.

The resulting efficiencies for anti-k_t jets with $R = 0.4$ for the two selection criteria are shown as a function of η for $p_{\mathrm{T}} > 100$ GeV in Figure 8. The jet quality selection efficiency of the Loose selection is greater than 99.9% over all η bins except in one bin at very high η. The Tight selection efficiency is lower in the central-η region due to the cut on $f_{\mathrm{ch}}/f_{\mathrm{max}}$. Otherwise, the Tight selection has $> 99.5\%$ efficiency over all η bins except in one bin at very high η.

Similarly, Figure 9 shows the jet quality selection efficiencies[6] as a function of p_{T} for various η ranges. The jet quality selection efficiency of the Loose selection is greater than 99.5% over all p_{T} bins. The Tight selection efficiency is lower in the central-η region due to the cut on $f_{\mathrm{ch}}/f_{\mathrm{max}}$. Otherwise, the Tight selection has an efficiency greater than 95% over all p_{T} bins. Jet quality selection efficiencies in data are compared to the simulation and ve good agreement is observed.

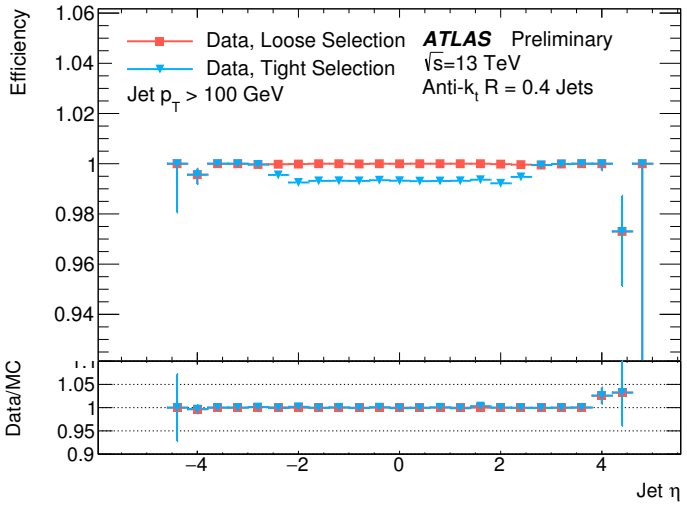

Figure 8: *Jet quality selection efficiency for anti-k_t jets with $R = 0.4$ measured with a tag-and-probe technique as a function of η for $p_T >$100 GeV, for the Loose and Tight selection criteria. Only statistical uncertainties are shown. The lower portion of the figure shows ratios of efficiencies measured in data and Monte Carlo simulation (*Pythia8*).*

[6] It should be noted that for jets with $p_{\mathrm{T}} < 50$ GeV and within the tracker acceptance, additional criteria were designed to select jets from the hard-scatter and to reject pile-up jets using the jet-vertex-tagger described in Reference [19]. When this tagger is employed, an inefficiency at selecting signal jets is introduced which is of the order of 10% for p_{T} =20 GeV. The jets rejected by this tagger have a large overlap with those rejected by the f_{ch}/f_{max} requirement of the tight selection, making the efficiency of the tight cut close to 100% at 20 GeV for jets selected using the jet-vertex-tagger.

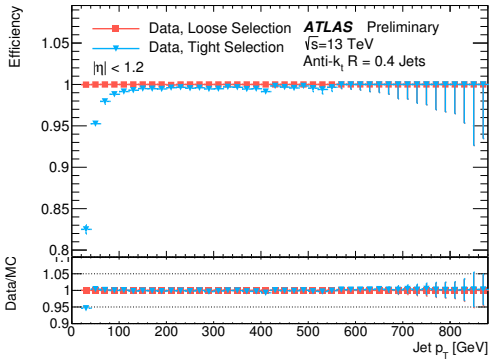

(a) $|\eta|$ <1.2

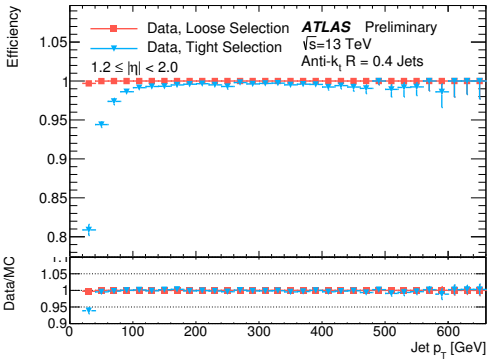

(b) 1.2≤ $|\eta|$ <2

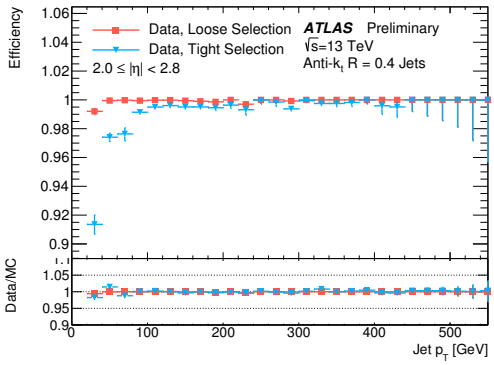

(c) 2≤ $|\eta|$ <2.8

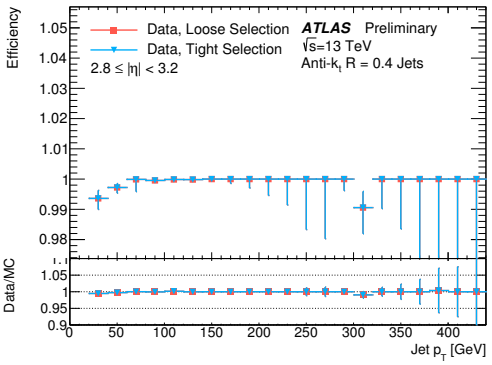

(d) 2.8≤ $|\eta|$ <3.2

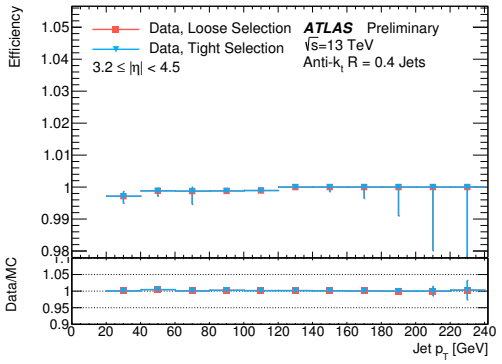

(e) 4.2≤ $|\eta|$ <4.5

Figure 9: *Jet quality selection efficiency for anti-k_t jets with $R = 0.4$ measured with a tag-and-probe technique as a function of p_T in η ranges, for the Loose and Tight selection criteria. Only statistical uncertainties are shown. The lower portion of the figure shows ratios of efficiencies measured in data and Monte Carlo simulation (*Pythia8*).*

8 Conclusion

The performance of the jet selection is studied using data recorded by the ATLAS experiment in $\sqrt{s}$ = 13 TeV proton–proton collisions, with a total integrated luminosity of 7 pb^{-1}. Quality criteria for the selection of reconstructed anti-k_t jets with $R = 0.4$ in the ATLAS detector are described, and two sets of selection are defined. The Loose selection is designed to provide an efficiency of selecting jets from proton-proton collisions above 99.5% for $p_{\mathrm{T}} > 20$ GeV, while the Tight selection is designed to further reject background jets for analyses sensitive to non-collision backgrounds with an efficiency at selecting jets from proton-proton collisions above 95% for $p_{\mathrm{T}} > 20$ GeV. Jets with p_{T} above 100 GeV are selected with larger than 99.9% and 99.5% efficiency for the Loose and Tight selections, respectively.

References

[1] ATLAS Collaboration, *Characterisation and mitigation of beam-induced backgrounds observed in the ATLAS detector during the 2011 proton–proton run*, JINST **8** (2013) P07004, arXiv: 1303.0223 [hep-ex].

[2] ATLAS Collaboration, *Jet energy measurement with the ATLAS detector in proton–proton collisions at $\sqrt{s}$ = 7 TeV*, Eur. Phys. J. C **73** (2013) 2304, arXiv: 1112.6426 [hep-ex].

[3] ATLAS Collaboration, *Monitoring and data quality assessment of the ATLAS liquid argon calorimeter*, JINST **9** (2014) P07024, arXiv: 1405.3768 [hep-ex].

[4] ATLAS Collaboration, *The ATLAS Experiment at the CERN Large Hadron Collider*, JINST **3** (2008) S08003.

[5] ATLAS Collaboration, *Operation and performance of the ATLAS semiconductor tracker*, JINST **9** (2014) P08009, arXiv: 1404.7473 [hep-ex].

[6] T. Sjostrand, S. Mrenna and P. Z. Skands, *A Brief Introduction to PYTHIA 8.1*, Comput.Phys.Commun. **178** (2008) 852–867, arXiv: 0710.3820 [hep-ph].

[7] R. Corke and T. Sjostrand, *Improved Parton Showers at Large Transverse Momenta*, Eur.Phys.J. **C69** (2010) 1–18, arXiv: 1003.2384 [hep-ph].

[8] B. Andersson et al., *Parton Fragmentation and String Dynamics*, Phys.Rept. **97** (1983) 31–145.

[9] ATLAS Collaboration, *ATLAS Pythia 8 tunes to 7 TeV data*, ATL-PHYS-PUB-2014-021, 2014, URL: http://cdsweb.cern.ch/record/1966419.

[10] ATLAS Collaboration, *The ATLAS Simulation Infrastructure*, Eur. Phys. J. C **70** (2010) 823, arXiv: 1005.4568 [hep-ex].

[11] S. Agostinelli et al., *GEANT4: A Simulation toolkit*, Nucl.Instrum.Meth. **A506** (2003) 250–303.

[12] G. Folger and J. Wellisch, *String parton models in GEANT4*, eConf **C0303241** (2003) MOMT007, arXiv: nucl-th/0306007 [nucl-th].

[13] M. Cacciari, G. P. Salam and G. Soyez, *The Anti-k(t) jet clustering algorithm*, JHEP **0804** (2008) 063, arXiv: 0802.1189 [hep-ph].

[14] ATLAS Collaboration, 'Jet Calibration and Systematic Uncertainties for Jets Reconstructed in the ATLAS Detector at $\sqrt{s}$ = 13 TeV (forthcoming)', tech. rep.

[15] ATLAS Collaboration, 'Performance of the ATLAS Inner Detector Track and Vertex Reconstruction in the High Pile-Up LHC Environment', tech. rep. ATLAS-CONF-2012-042, CERN, 2012.

[16] M. Cacciari, G. P. Salam and G. Soyez, *The Catchment Area of Jets*, JHEP **0804** (2008) 005, arXiv: 0802.1188 [hep-ph].

[17] ATLAS Collaboration, *Readiness of the ATLAS liquid argon calorimeter for LHC collisions*, Eur. Phys. J. C **70** (2010) 723, arXiv: 0912.2642 [hep-ex].

[18] ATLAS Collaboration, *Search for new phenomena in final states with an energetic jet and large missing transverse momentum in pp collisions at $\sqrt{s}$ = 8 TeV with the ATLAS detector* (2015), arXiv: 1502.01518 [hep-ex].

[19] ‘Tagging and suppression of pileup jets with the ATLAS detector’, tech. rep. ATLAS-CONF-2014-018, CERN, 2014, URL: https://cds.cern.ch/record/1700870.